CHEESA: Chemical Engineering Research Articles
ISSN 2614-8757 (Print), ISSN 2615-2347 (Online)
Homepage: https://e-journal.unipma.ac.id/index.php/cheesa

CHEESA, 9(1), pp 64-76, 2026

Binary System Adsorption of Methylene Blue and Congo Red Using Magnetic Activated Carbon

Tarikh Azis Ramadani[1*)], Yusron Khoiru Nadhori[2)], Novi Eka Mayangsari[2)], Alma Vita Sophia[3)], Indah Permata Sari[2)]

[1)]Politeknik Perkapalan Negeri Surabaya, Department of Shipbuilding Engineering, Jalan Teknik Kimia, Kampus ITS Sukolilo, Surabaya, Indonesia
[2)]Politeknik Perkapalan Negeri Surabaya, Department of Waste Treatment Engineering, Jalan Teknik Kimia, Kampus ITS Sukolilo, Surabaya, Indonesia
[3)]Politeknik Perkapalan Negeri Surabaya, Department of Business Management, Jalan Teknik Kimia, Kampus ITS Sukolilo, Surabaya, Indonesia

*corresponding author: tarikh@ppns.ac.id

Article History

Submitted: 29th June 2026; Revised: 21th September 2026; Accepted: 25th September 2026; Available online: 10th October 2026; Published Regularly: June 2026

doi: 10.25273/cheesa.v9i1.25102.64-76

Abstract

Dye pollution is an environmental concern posing significant risks to human health and water quality, showing the need for effective methods to reduce dye concentrations in contaminated water. Therefore, this study aimed to explore the reduction of dye concentration in a binary system through adsorption using magnetic activated carbon derived from durian peel. To assess the properties relevant to adsorption, the adsorbent was characterized using Fourier Transform Infrared Spectroscopy (FTIR), Scanning Electron Microscopy coupled with Energy-Dispersive X-ray Spectroscopy (SEM-EDX), X-ray Diffraction (XRD), Vibrating Sample Magnetometry (VSM), and Brunauer–Emmett–Teller Analysis (BET). The adsorption process was evaluated based on contact time, dose, and pH. The results showed that the reduction in the concentrations of Methylene Blue (MB) and Congo Red (CR) was influenced by contact time, dose, and pH, with an efficiency of approximately 97%. The observed behavior was best described by the pseudo-second-order kinetic model and Langmuir isotherm for MB and CR removal, respectively. However, intraparticle diffusion had no effect on the adsorption process because the C value was greater than 0. This study showed that magnetic activated carbon derived from durian peel possessed promising potential as an effective adsorbent for reducing dye concentration in a binary system.

Keywords: adsorption; binary system; congo red; durian peel; methylene blue

1. Introduction

Environmental pollution is a problem faced by many countries due to industrial growth, as various activities generate hazardous substances capable of entering water bodies. One of the hazardous substances released is synthetic dye, which is often produced by the textile, printing, dyeing, and paper industries [1]. The release of large amounts of synthetic dye can inhibit photosynthesis, disrupt aquatic ecosystems, and reduce water quality [2]. Exposure to these pollutants causes several diseases in humans, such as coughing, stomachache, vomiting, bleeding, infection, and cancer, even at low concentrations [3]. Consequently, several mitigation efforts have been implemented to reduce the persistence of various synthetic dyes such as methylene blue (MB) and Congo red (CR) in industrial wastewater [4], alongside their complex chemical structures and low natural degradability [5].

The environmental impact of synthetic dyes has led to the development of various wastewater treatment methods, including coagulation-flocculation, ion exchange, chemical-biological degradation, electrochemical degradation, and biological processes [6]. Among these methods, adsorption has been considered most effective due to low cost, flexibility, and ease of operation [7]. Adsorption requires a mass-separation agent to reduce dye concentration. Although commercial

This is an open access article under the CC BY license (http://creativecommons.org/licenses/by/4.0/)

activated carbon is commonly used as an adsorbent to reduce dye concentration in wastewater, its application is hindered by high production and regeneration costs, limited selectivity, and reduced reusability [8]. Consequently, several studies have focused on identifying sustainable adsorbents derived from lignocellulosic agricultural biomass [9], such as durian (*Durio zibethinus* Murr.) [10]. Durian is a fruit commonly found in Southeast Asia, including in Indonesia, where the large quantity of peel (60-75% of the fruit) generated after consumption presents a considerable waste-management challenge [11]. Environmental pollution, pest attraction, and disposal challenges attributed to bulky size and slow rate of decomposition are concerns arising from improper management of durian peels [12]. However, durian peel has potential as an adsorbent due to its lignocellulosic composition, comprising 50–60% cellulose, 30.7% hemicellulose, 13.6% lignin, and 5% starch [10],[13].

Activated carbon is an adsorbent produced from lignocellulose through physical or chemical activation methods [14]. This material has characteristics such as a high specific surface area with a well-developed pore structure, contains a significant amount of O and N functional groups, and features heteroatoms on the surface of the activated carbon [15]. However, adsorbents derived from lignocellulosic agricultural biomass face challenges in separation from aqueous solution and subsequent reuse compared to commercial activated carbon [16]. These challenges are associated with increased costs and potential adverse environmental effects [16], which can be addressed by incorporating metal oxide nanomaterials, particularly magnetic nanoparticles. Metal oxide nanomaterials show magnetic properties due to the presence of magnetite (Fe_3O_4) and can be attributed to the surface of activated carbon through a coprecipitation method [17],[18]. The addition of these materials has been reported to enhance mechanical strength, promote regeneration, improve adsorption capacity, and facilitate reuse [19]. Therefore, activated carbon combined with magnetic properties retains the chemical and physical properties of activated carbon while maintaining magnetic separation characteristics [20]. These combined properties support the use of magnetic activated carbon in reducing various pollutants, such as heavy metals and dyes [15].

Despite the numerous previous reports, the simultaneous removal of dyes using magnetic activated carbon in a binary system has not been extensively explored. Therefore, this study aims to simultaneously remove MB and CR in a binary system by preparing magnetic activated carbon from durian peel. The characteristics of the adsorbent are explored through Fourier Transform Infrared Spectroscopy (FTIR), Scanning Electron Microscopy with Energy-Dispersive X-ray Spectroscopy (SEM-EDX), X-ray Diffraction (XRD), Vibrating Sample Magnetometer (VSM), and Brunauer-Emmett-Teller (BET) analyses. The ability of the adsorbent was evaluated based on contact time, dose, and pH, including reusability. Additionally, a comprehensive understanding of the adsorption mechanism was reviewed based on adsorption isotherms and kinetics.

2. Research Methods

2.1 Materials

This study used durian peels as raw materials for adsorbents obtained from local markets in Surabaya, Indonesia. Other materials included iron (III) chloride hexahydrate ($FeCl_3.6H_2O$, MW: 270.30 g/mol, 97% from Sigma-Aldrich), iron (II) sulfate heptahydrate ($FeSO_4.7H_2O$, MW: 278.01 g/mol, 99% from Sigma-Aldrich), sodium hydroxide (NaOH pellets, 99% from Supelco), CR ($C_{32}H_{22}N_6Na_2O_6S_2$, MW: 696.66 g/mol), and MB ($C_{16}H_{18}ClN_3S.xH_2O$, MW: 319.85 g/mol). Additionally, deionized water was used in all study procedures.

2.2 Synthesis of the activated carbon

The production of activated carbon used in this study followed the procedures described in the literature with slight modifications [10]. The durian peel was washed, cut into 3 cm pieces, and dried in the sun for 24 hours. This was followed by carbonization in a furnace at 320°C for 2 hours, and the peel was placed in a desiccator, reduced to powder, and strained through a 100-mesh sieve. The solid powder charcoal was activated in 0.5 M NaOH at a solid-to-liquid ratio of 1:10 for 24 hours. Subsequently, the activated carbon was filtered, rinsed to a neutral pH, and dried at 120°C for 30 minutes.

2.3 Synthesis of the magnetic activated carbon (Fe_3O_4@AC)

The synthesis of magnetic activated carbon followed the general procedure reported in the literature [21]. Initially, 10 g of activated carbon was

blended with 7.32 g of $FeCl_3{\cdot}6H_2O$ and 13.32 g of $FeSO_4{\cdot}7H_2O$, and 400 mL of deionized water was added. The process was carried out at 60°C under stirring, cooled to 40°C, and the solution was adjusted to pH 10-11. Furthermore, the suspension was stirred for 4 hours and left to settle overnight. The solid product was separated from the solution, rinsed until neutral, and impurities were rinsed with ethanol and acetone. The product was dried for 48 hours at 60°C.

2.4 Material characterization

Characterization was used to describe the properties of the adsorbent. The functional groups of the material before and after the adsorption process were identified using FTIR, Thermo Scientific Nicolet iS10. The material was characterized before and after the adsorption process using SEM-EDX, FEI Inspect S50. The crystalline phase of the material was characterized using XRD (XPert PRO, PANalytical). A VSM, Quantum Design PPMS VersaLab Cryogen-free 3 Tesla, was used to characterize the material's magnetic properties. The Brunauer-Emmett-Teller (BET, TMAXCN BSD-PSI) method was used to measure the specific surface area of the adsorbent.

2.5 Adsorption experiment

The removal of MB and CR was evaluated using several parameters, including contact time (20 min, 40 min, 60 min, 80 min, 100 min), dose (0.25 g, 0.5 g, 0.75 g, 1 g, 1.25 g), and pH (2, 6, 10). The system used a 50:50 volume ratio of MB and CR, with each dye having a concentration of 100 ppm. The concentrations of MB and CR in a binary system were measured using a UV-Vis spectrophotometer at the maximum wavelength. In a binary system, the dye concentration was calculated using Equation 1 and Equation 2 [22].

$$C_{MB} = \frac{k_{BCR}d_{MB} - k_{BMB}d_{CR}}{k_{AMB}k_{BCR} - k_{ACR}k_{BMB}} \quad \textbf{.....(Equation 1)}$$

$$C_{CR} = \frac{k_{AMB}d_{CR} - k_{ACR}d_{MB}}{k_{AMB}k_{BCR} - k_{ACR}k_{BMB}} \quad \textbf{.....(Equation 2)}$$

$$Adsorption\ capacity\ \left(\frac{mg}{g}\right) = \frac{(C_0 - C_t)V}{m} \quad \textbf{..(Equation 3)}$$

$$Removal\ (\%) = \frac{(C_0 - C_t)}{C_0} \times 100\% \quad \textbf{.....(Equation 4)}$$

The constants k_{AMB}, k_{BMB}, k_{ACR}, and k_{BCR} refer to the calibration coefficients of MB and CR at the selected wavelengths of 661 and 498 nm, respectively. Optical density measurements are represented by d_{MB} and d_{CR}. The adsorption performance of MB and CR was evaluated using Equation 3 and Equation 4, taking into account the initial concentration (C_0), concentration at time t (C_t), adsorbent mass (m), and solution volume (V).

Additionally, the adsorbent was subjected to four reuse cycles to assess stability in dye removal. Each cycle was conducted at an initial concentration of 100 ppm, with an adsorbent dose of 0.25 g and a contact time of 60 minutes.

2.6 Adsorption isotherms

Adsorption isotherms were used to evaluate the equilibrium relationship between the liquid and solid phases based on the Langmuir, Freundlich, and Temkin models, as presented in Equation 5, Equation 6, and Equation 7, respectively [23]. The parameter q_m shows the monolayer adsorption capacity, expressed in mg/g, while K_L represents the Langmuir equilibrium constant (L/mg). For the Freundlich isotherm, the constants are denoted by K_F ($L^{1/n}.mg^{1-1/n}.g^{-1}$) and n, while the Temkin model constants are represented by A ($L.g^{-1}$) and b ($J.mol^{-1}$).

$$\frac{C_e}{q_e} = \frac{1}{q_m K_L} + \frac{C_e}{q_m} \quad \textbf{.....(Equation 5)}$$

$$\ln q_e = \frac{1}{n}\ln C_e + \ln K_F \quad \textbf{.....(Equation 6)}$$

$$q_e = \frac{RT}{b}\ln(AC_e) \quad \textbf{.....(Equation 7)}$$

$$\ln(q_e - q_t) = \ln q_e - k_1 t \quad \textbf{.....(Equation 8)}$$

$$\frac{t}{q_t} = \frac{1}{k_2 q_e^2} + \frac{1}{q_e} \quad \textbf{.....(Equation 9)}$$

$$q_t = k_p t^{0.5} + B \quad \textbf{.....(Equation 10)}$$

2.7 Adsorption kinetics

Adsorption kinetics were used to describe adsorption rates, adsorbent performance, and mass-transfer mechanisms. These parameters were evaluated using pseudo-first-order diffusion (Equation 8), pseudo-second-order diffusion (Equation 9), and intra-particle diffusion (Equation 10) [25]. The adsorption capacity at equilibrium and time t are denoted by q_e and q_t, respectively, both expressed in mg/g. Meanwhile, k_1, k_2, and k_p correspond to the rate constants of the pseudo-first-order, pseudo-second-order, and intra-particle diffusion kinetic models, respectively.

3. Results and Discussion

Material characterization was performed to evaluate the physicochemical properties of the adsorbent and its potential for dye removal from a binary system. This study used FTIR, SEM-EDX, XRD, VSM, and BET characterization methods to assess the ability of Fe_3O_4@AC material to reduce dyes in a binary system. Figure 1.a shows the FTIR spectra for the Fe_3O_4@AC material before and after the adsorption process. Before adsorption, the material showed distinct intensity peaks in the spectral range around 3350 cm^{-1}, 2920 cm^{-1}, 2100 cm^{-1}, 1580 cm^{-1}, 1040 cm^{-1}, and 550 cm^{-1}. The peak at 3350 cm^{-1} was associated with O–H stretching vibrations [20], while 2920 cm^{-1} showed aliphatic C–H stretch [24]. The triple bond between carbon atoms in the alkyne group was detected by peaks in the spectral range of 2100 cm^{-1} [25]. The band located around 1580 cm^{-1} corresponded to C=O bonds [26], while C–O stretching vibration was shown in the 1040 cm^{-1} range [21]. The material contained Fe–O functional groups, as shown by the existence of a peak in the range of 550 cm^{-1} [27]. After adsorption, several significant changes were observed in FTIR spectra (Figure 1.a). The C=O functional group shifted by approximately 1590–1570 cm^{-1}, showing an interaction between the carbonyl groups on the carbon surface and the MB and CR [28],[29]. Interactions between the C–O functional groups and the dye molecules were also shown by a shift in the FTIR spectra around 1040 cm^{-1} [29],[30]. These interactions contributed to electrostatic attraction between the adsorbent surface and the MB and CR molecules [31].

Figure 1.b shows the XRD results before and after adsorption. The material appeared to contain Fe_3O_4@AC microcrystals and an irregular layered graphite structure, as indicated by the amorphous diffraction peak at 26.18° (002) between 25° and 30° [32]. The crystal surface of the graphite structure (100) was shown by a peak at 43.46° [33]. Furthermore, the main diffraction peaks of Fe_3O_4 for the (220), (311), (511), and (440) crystal planes were shown by several peaks at 30.24°, 35.70°, 57.37°, and 63.07°. These planes are consistent when compared with JCPDS No. 33-0665 [20], showing that the Fe_3O_4 core remains crystalline [34]. Magnetic activated carbon has been successfully synthesized and characterized by the (311) crystal plane, which exhibits a higher peak intensity.

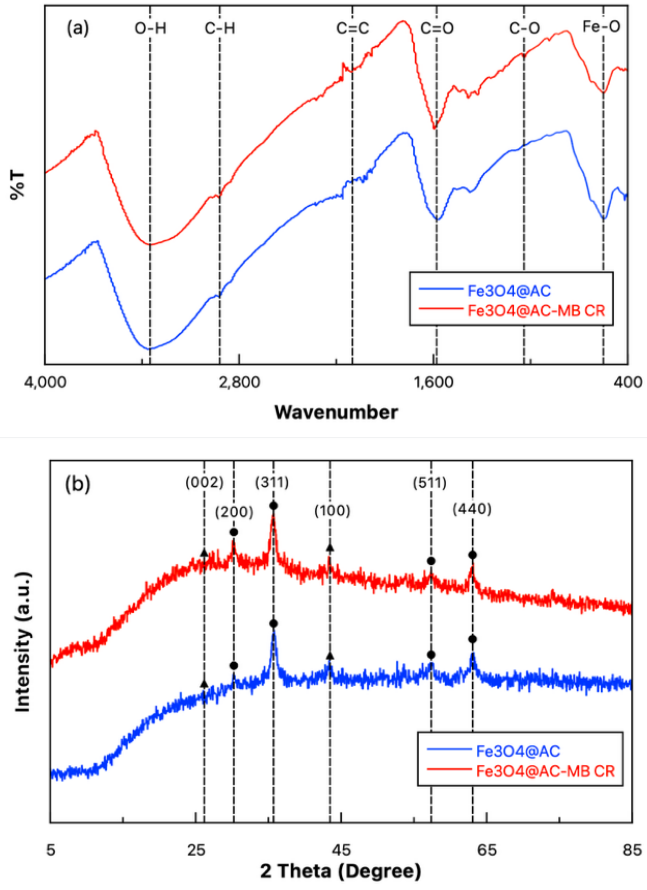


Figure 1. (a) Fourier Transform Infrared (FTIR) spectra and (b) X-ray Diffraction (XRD) of magnetic activated carbon (Fe_3O_4@AC) before adsorption and after adsorption of Methylene Blue (MB) and Congo Red (CR) (Fe_3O_4@AC-MBCR). The C=O and C-O functional groups shifted, showing an interaction between the carbonyl groups on the carbon surface and the MB and CR.

The morphological characteristics of the material were evaluated using SEM at magnifications of 2500x and 10000x, as presented in Figure 2. Based on observation, the adsorbent showed an uneven shape with varying sizes and pores that appeared dense and evenly distributed. The adsorption process caused pore filling, thereby decreasing pore size, as confirmed by EDX analysis, which determined the elemental composition of the material. As presented in Figure 3, the elements Fe, C, and O were the main components of the Fe_3O_4@AC. The presence of Fe showed that the material possessed magnetic properties [35], while C and O contributed to the occurrence of electrostatic interactions with the adsorbent and the dye [31]. The adsorption process also increased the concentrations of C and O, showing that the dye had been successfully adsorbed onto the adsorbent surface. Additionally, the material contained several inorganic species, such as small amounts of the elements Si and Mg, which could be considered impurities. Inorganic species were also found in several related studies [36],[37].

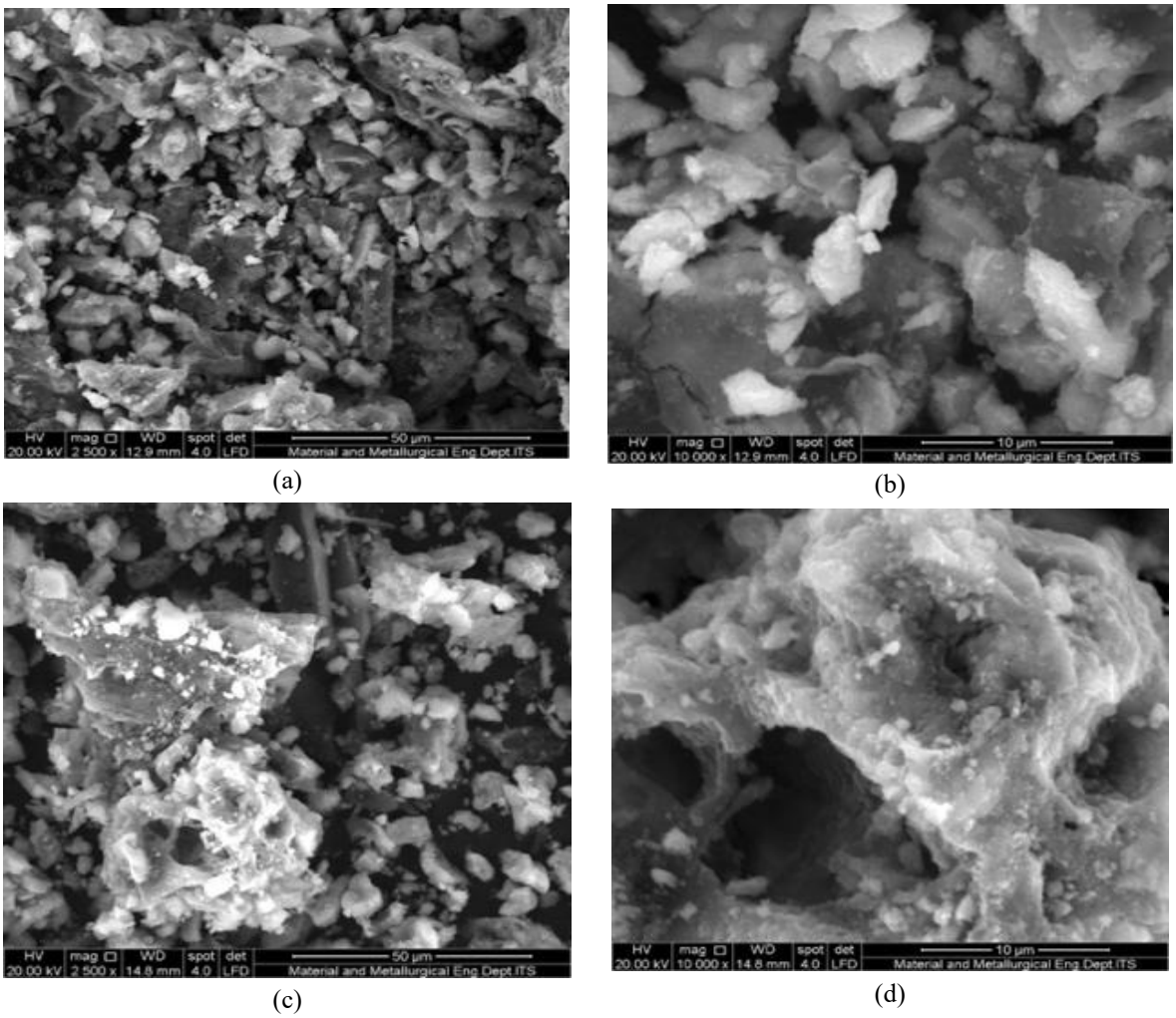
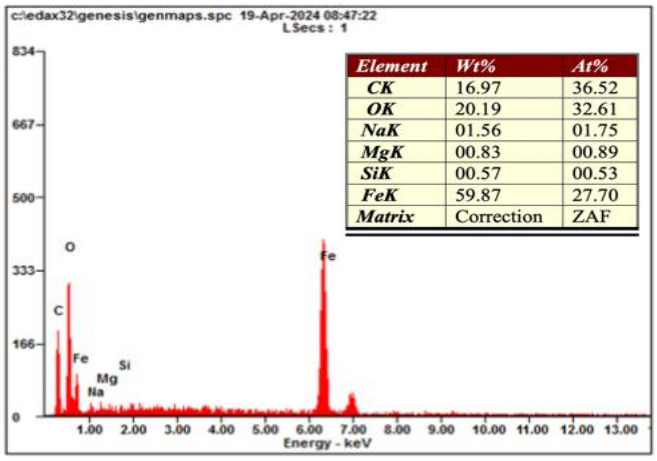
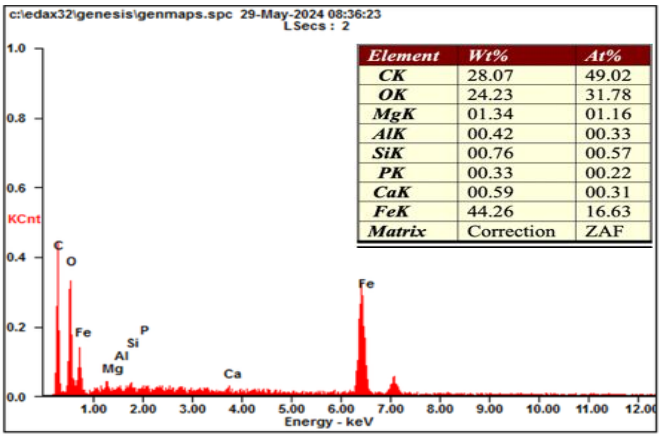


Figure 2. Scanning Electron Microscope (SEM) images, (a) magnetic activated carbon (Fe_3O_4@AC) before adsorption at magnification power 2500x and (b) 10000x, (c) after adsorption of Methylene Blue (MB) and Congo Red (CR) (Fe_3O_4@AC-MBCR) at magnification power 2500x and (d) 10000x. The adsorption process led to pore filling, thereby reducing the pore size.



(a)



(b)

Figure 3. Energy-dispersive X-ray (EDX) analysis of (a) magnetic activated carbon (Fe_3O_4@AC) before adsorption and (b) after the adsorption of Methylene Blue (MB) and Congo Red (CR) (Fe_3O_4@AC-MBCR). The results showed an increase in the C and O contents after adsorption, indicating the successful adsorption of MB and CR onto the adsorbent surface.

Table 1. Brunauer-Emmett-Teller (BET) analysis of magnetic activated carbon (Fe_3O_4@AC) before adsorption

Material	Pore size (nm)	Pore volume (cc/g)	Specific surface area (m^2/g)
Fe_3O_4@AC	4.3552	0.131226	60.2614

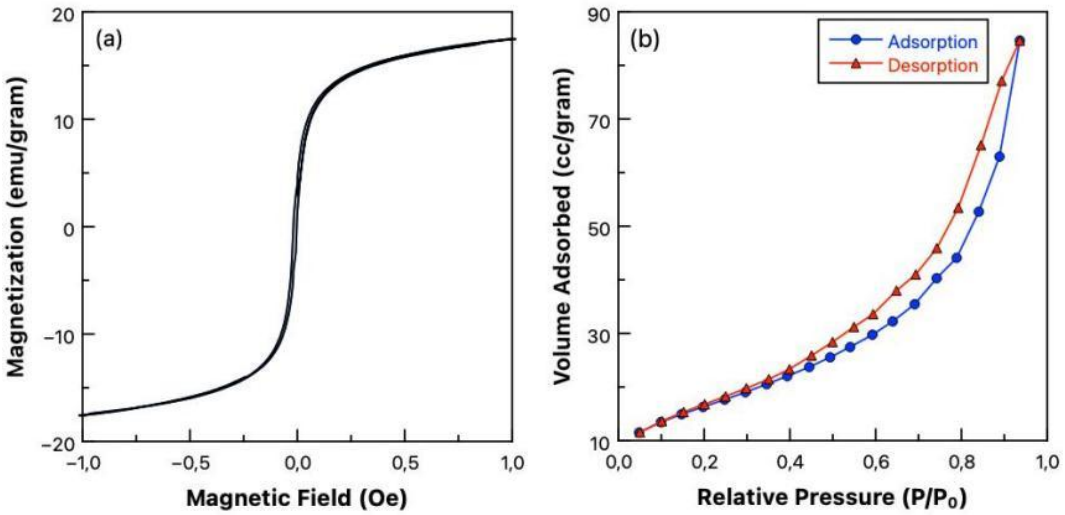


Figure 4. (a) Vibrating Sample Magnetometer (VSM) analysis of magnetic activated carbon (Fe_3O_4@AC) showing a saturation magnetization (M_s) of 17.6 emu/g and a remanent magnetization (M_r) of 4.156 emu/g; and (b) an adsorption isotherm for gas-solid equilibrium classified as Type V for magnetic activated carbon (Fe_3O_4@AC)

Based on the magnetization curve presented in Figure 4.a, the saturation magnetization (Ms) and remanence (Mr) of the sample were 17.6 emu/g and 4.156 emu/g, respectively. The ferromagnetism was determined according to the ratio of saturation magnetization to remanence, which showed superparamagnetic behavior at room temperature because the ratio was below 25% [38]. Based on the magnetization curve, the material was also classified as a soft magnetic material [35]. In addition to the magnetic properties, the textural characteristics of Fe_3O_4@AC were evaluated using the BET method, with pore size, pore volume, and specific surface area presented in Table 1. The adsorbent material had a specific surface area of 60.2614 m^2/g and was classified as mesoporous because of the pore sizes ranging from 2 nm to 50 nm [39]. The pore structure supported pore filling by MB and CR, which have molecular sizes of 1.43 and 2.62 nm, respectively [40]. Additionally, adsorption isotherms for gas-solid equilibria were determined based on the N_2 adsorption-desorption isotherm profile, and the system was classified as type V, as presented in Figure 4.b [41].

The effect of contact time on dye adsorption was investigated by varying the contact time from 20 to 100 min at 20-min intervals, with an initial dye concentration of 100 ppm, an adsorbent dose of 1 g, and an MB ratio of 50:50. Figure 5a shows the effect of contact time on the simultaneous adsorption of MB and CR. Rapid adsorption occurred during the initial stage, followed by a gradual decrease in adsorption rate as the system reached equilibrium at 80 min. This observed trend could be attributed to the abundance of available adsorption sites on the adsorbent surface for MB and CR. As the process progressed, the number of available sites gradually decreased, leading to a lower adsorption rate as the system approached equilibrium [39]. Therefore, the adsorption efficiency decreased with increasing contact time after reaching equilibrium.

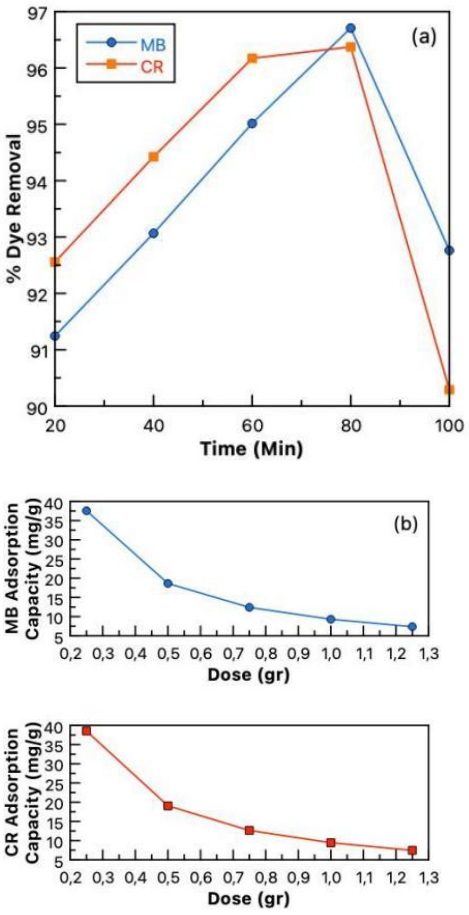
Following the determination of the equilibrium contact time, the effect of adsorbent dose on dye adsorption was investigated by varying the dose from 0.25 to 1.25 g at 0.25-g intervals, using an initial dye concentration of 100 ppm, an adsorption time of 40 min, and an MB ratio of 50:50. As shown in Figure 5b, increasing the adsorbent dose increased the simultaneous removal of MB and CR. In comparison, adsorption capacity decreased as the adsorbent dose increased. This showed an inverse relationship between adsorbent dose and adsorption capacity. The decrease in adsorption capacity may be attributed to increased competition between MB and CR for the available adsorption sites as the amount of adsorbent increased [42]. Since the concentrations of MB and CR in the solution remain constant after reaching adsorption equilibrium, the amounts of MB and CR decrease [43]. This leads to a decrease in adsorption per unit of Fe_3O_4@AC with increasing adsorbent dose, as similarly observed in previous related studies [20],[42].

The adsorption behavior of MB and CR was evaluated by monitoring changes in pH at an initial concentration of 100 ppm, an adsorbent dose of 0.8 g, and an MB-CR mixture in a 50:50 ratio. Figure 5(c) shows the effect of pH on the removal efficiencies of MB and CR in the binary system. The results showed that MB removal efficiency increased with higher pH, rising from approximately 95.9% at pH 2 to 99.1% at pH 10. In comparison, CR removal efficiency decreased as the pH increased, declining from approximately 98.5% at pH 2 to 92.4% at pH 10. The increase in alkalinity enhanced the deprotonation of surface functional groups, such as –COOH and Fe–OH, leading to the formation of negatively charged $–COO^-$ and $Fe–O^-$ species, respectively [44],[45]. Electrostatic interactions occurred between the functional groups and the cationic MB molecules [46].

Under acidic conditions, the increased concentration of H_3O^+ ions resulted in competition between H_3O^+ and MB molecules for available adsorption sites, thereby reducing MB removal efficiency [42]. As the pH increased, this competition was reduced, favoring the adsorption of MB molecules and consequently increasing MB removal efficiency. In comparison, the removal efficiency of CR showed the opposite trend. When the pH was shifted toward acidic conditions, the efficiency of CR removal in a binary system with MB tended to increase. According to previous studies, acidic conditions induced dissociation of the sulfonate groups present in CR, leading to the formation of $–SO_3^-$ under acidic conditions. This phenomenon enhanced electrostatic interactions between the adsorbent and the CR molecules, thereby promoting stronger adsorption. Additionally, the reduction of OH^- ions in the system reduced competition for adsorption sites, thereby increasing the efficiency of CR removal [22]. A similar phenomenon has also been reported in several previous studies [5],[22],[47].

The interaction between the adsorbent and the adsorbate was explored using an isotherm adsorption model, as presented in Figure 6. The Langmuir model provided information regarding monolayer adsorption, while the Freundlich model explained the role of the material's functional groups in the adsorption process. The Temkin model described chemical adsorption. The MB removal process showed that the Langmuir model (R^2=0.8728) produced better results than the Freundlich (R^2=0.8506) and Temkin models (R^2=0.8115). Regarding CR, the Langmuir (R^2=0.9657) and Freundlich models (R^2=0.9659) provided comparable fits to the experimental equilibrium data compared to the Temkin model (R^2=0.8969). Additionally, adsorption kinetics were evaluated to assess the effectiveness of the material in dye removal using pseudo-first-order, pseudo-second-order, and intraparticle diffusion models (Figure 7). The adsorption of MB and CR tended toward the pseudo-second-order model, as indicated by the correlation coefficients, with R^2 values of 0.999 and 0.998, respectively. This shows that the removal of MB and CR was influenced by the number of active sites on the adsorbent surface [48]. Intraparticle diffusion was also evaluated, and the results showed kMB and kCR values of 0.1982 mg/g·min$^{0.5}$ and 0.1144 mg/g·min$^{0.5}$, with R^2 values of 0.997 and 0.990 for MB and CR, respectively. Furthermore, the influence of the boundary layer on the adsorption process was assessed from the intercept values of the intraparticle diffusion model. The adsorption process yielded CMB and CCR values of 11.123 and 8.604, respectively, showing that intraparticle diffusion did not control the adsorption process because the C values were not equal to 0 [20]. The high C values show a greater contribution from the boundary layer to the overall adsorption process [49].

Reusability tests were conducted to assess stability and practical performance using an initial concentration of 100 ppm for each dye, a dose of 0.25 g, a contact time of 60 minutes, and a 50:50 mixture of MB and CR. The results presented in Figure 8 showed that increasing the number of reuse cycles progressively decreased the removal efficiency of the adsorbent in the binary system. The reusability tests showed that the material maintained a dye removal efficiency above 75% after 4 cycles. Additionally, the decrease in efficiency with each cycle was caused by the gradual depletion of active sites in the adsorbent, which led to a decline in the adsorbent's ability to reduce pollutants [50].



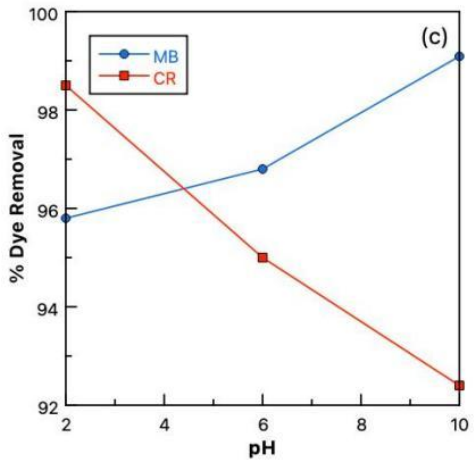


Figure 5. Adsorption of Methylene Blue (MB) and Congo Red (CR) in a binary system as a function of (a) contact time (20–100 min), (b) adsorbent dose (0.25–1.25 g), and (c) pH (2–10)

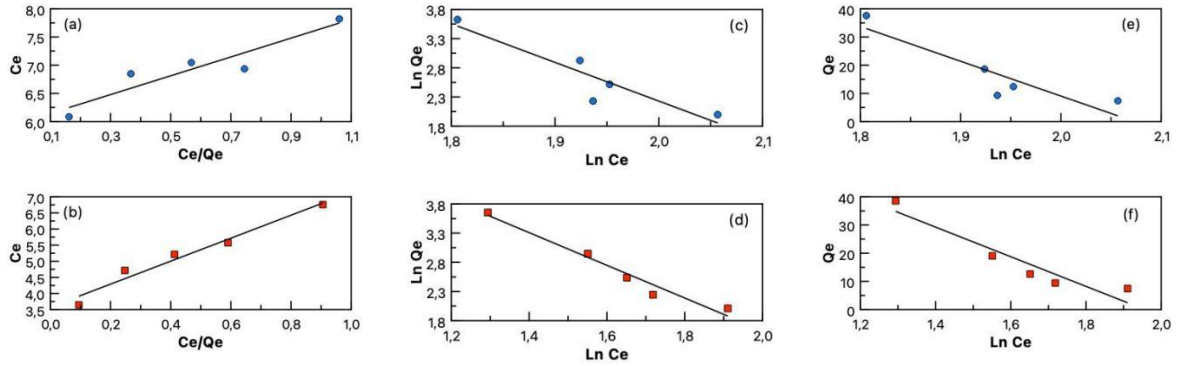


Figure 6. Adsorption isotherm plots for the Langmuir model: (a) Methylene Blue (MB) with R^2=0.8728 and (b) Congo Red (CR) with R^2=0.9657; the Freundlich model: (c) Methylene Blue (MB) with R^2=0.8506 and (d) Congo Red (CR) with R^2=0.9659; and the Temkin model: (e) Methylene Blue (MB) with R^2=0.8115 and (f) Congo Red (CR) with R^2=0.8969

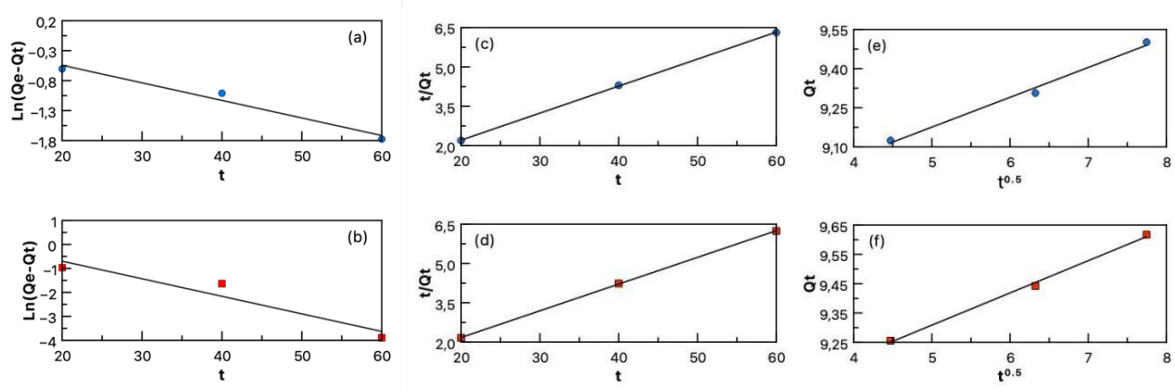


Figure 7. Adsorption kinetics plots for pseudo-first-order model: (a) Methylene Blue (MB) with R^2=0.9694 and (b) Congo Red (CR) with R^2=0.9109; pseudo-second-order model: (c) Methylene Blue (MB) with R^2 0.9998 and (d) Congo Red (CR) with R^2 0.9999; intraparticle diffusion model: (e) Methylene Blue (MB) with R^2 0.9909 and (f) Congo Red (CR) with R^2 0.9968

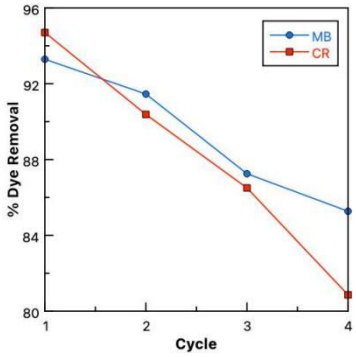


Figure 8. Methylene Blue (MB) and Congo Red (CR) removal efficiencies after a 4-cycle reuse test

4. Conclusion

In conclusion, this study shows that magnetic activated carbon derived from durian peel has been successfully synthesized. The material contains functional groups, a mesoporous structure, and magnetic properties that support the adsorption of dyes, achieving removal efficiencies of 99% for MB and 98% for CR. The decrease in dye concentration is influenced by contact time, adsorbent dose, and pH, which are associated with the interaction between the dyes and the adsorbent, including electrostatic forces. The adsorption isotherm results show that the Langmuir model is the best fit for the removal of MB and CR in the binary system, suggesting a monolayer adsorption process. Furthermore, the adsorption kinetics show that the

removal process follows a pseudo-second-order model. The process is not affected by intraparticle diffusion because the C parameter is not equal to 0. The material also maintains good performance after four cycles, achieving a separation efficiency of over 75%. In line with the analysis, this study shows that the material is an effective and promising adsorbent for removing dyes in a binary system.

AI Usage Statements

During the preparation of this manuscript, the authors used Grammarly (1.170.1.0, Superhuman) for correcting grammar, spelling, punctuation, and writing style in English. All AI-generated outputs were critically reviewed and thoroughly edited by the authors to ensure factual accuracy, clarity of expression, and compliance with academic standards. The authors take full responsibility for the integrity and content of this manuscript.

CRediT Authorship Statement

Tarikh Azis Ramadani: Writing – original draft, Supervision, Methodology, Investigation, Funding acquisition, Conceptualization. **Yusron Khoiru Nadhori:** Methodology, Investigation. **Novi Eka Mayangsari:** Writing – original draft, Methodology, Supervision, Investigation, Conceptualization. **Alma Vita Sophia:** Methodology, Writing – review & editing. **Indah Permata Sari:** Methodology, Investigation.

Declaration of competing interests

The authors declare that there are no conflicts of interest.

Acknowledgments

The authors are grateful to the PPNS DIPA for fiscal year 2026 (Contract No: 904/DST/PL19/PT.01.04/2026) for supporting this article

References

[1] Kumari, U. (2024). Textile Dyes and Their Impact on the Natural Environment (pp. 17–30). doi: 10.1007/978-981-97-5341-3_2

[2] Oladoye, P. O., Bamigboye, M. O., Ogunbiyi, O. D., & Akano, M. T. (2022). Toxicity and decontamination strategies of Congo red dye. *Groundwater for Sustainable Development*, 19, 100844. doi: 10.1016/j.gsd.2022.100844

[3] Phan, K.-H., Le, L.-T., Ninh, T.-T. N., Tran, C.-S., Nguyen, T.-T., Nguyen, D.-T.-D., … Bui, X.-T. (2024). Decolorization and degradation of azo dyes in thermophilic biological wastewater treatment process: A mini-review. *Case Studies in Chemical and Environmental Engineering*, 10, 101018. doi: 10.1016/j.cscee.2024.101018

[4] Lellis, B., Fávaro-Polonio, C. Z., Pamphile, J. A., & Polonio, J. C. (2019). Effects of textile dyes on health and the environment and bioremediation potential of living organisms. *Biotechnology Research and Innovation*, 3(2), 275–290. doi: 10.1016/j.biori.2019.09.001

[5] Chand, M., Kumawat, A., & Srivastava, S. (2026). Zeta potential-mediated comparative adsorption study of cationic (Methylene blue) and anionic (Congo red) dye onto spent tea (Camellia sinensis) leaves powder. *Surfaces and Interfaces*, 80, 108271. doi: 10.1016/j.surfin.2025.108271

[6] Abbas, S. H., Younis, Y. M., Rashid, K. H., & Khadom, A. A. (2022). Removal of methyl orange dye from simulated wastewater by electrocoagulation technique using Taguchi method: kinetics and optimization approaches. *Reaction Kinetics, Mechanisms and Catalysis*, 135(5), 2663–2679. doi: 10.1007/s11144-022-02269-9

[7] Nguyen, D. T. C., Jalil, A. A., Nguyen, L. M., & Nguyen, D. H. (2025). A comprehensive review on the adsorption of dyes onto activated carbons derived from harmful invasive plants. *Environmental Research*, 279, 121807. doi: 10.1016/j.envres.2025.121807

[8] El Meziani, S., Agnaou, H., El Haddaj, H., Boumya, W., Barka, N., & Elhalil, A. (2025). Sustainable adsorption technologies for textile dye removal: Advances in biomass-derived and magnetically modified activated carbons. *Cleaner Chemical Engineering*, 12, 100210. doi: 10.1016/j.clce.2025.100210

[9] Kassa, A., Engida, A., & Endaye, M. (2025). Eco-friendly adsorbents for industrial dye removal: A comprehensive review of low-cost alternatives. *Desalination and Water Treatment*, 323, 101362. doi: 10.1016/j.dwt.2025.101362

[10] Tambun, R., Haryanto, B., Alexander, V., Manurung, D. R., & Ritonga, A. P. (2024). Durian peel (Durio zibethinus) utilization as an adsorbent in the purification of acidified crude glycerol. *South African Journal of Chemical Engineering*, 49, 162–169. doi: 10.1016/j.sajce.2024.05.002

[11] Mulyati, A. H., Widyiastuti, D., & Muslimin, I. (2019). Characteristics of durian seed brownies which enriched with coconut flour. *Journal of Science Innovare*, 2(01), 06–09. doi: 10.33751/jsi.v2i01.1522

[12] Nguyen, P. A. T., Nguyen, T. T. T., & Vo, D. K. N. (2024). Pectin from durian peel (Durio zibethinus Murr.) - a novel reducing and stabilizing agent: Physicochemical properties, green synthesis of silver

nanoparticles and antimicrobial properties. *Carbohydrate Polymer Technologies and Applications*, 8, 100623. doi: 10.1016/j.carpta.2024.100623

[13] Lubis, R., Saragih, S. W., Wirjosentono, B., & Eddyanto, E. (2018). Characterization of durian rinds fiber (Durio zubinthinus, murr) from North Sumatera (p. 020069). doi: 10.1063/1.5082474

[14] Zeng, H., Zeng, H., Zhang, H., Shahab, A., Zhang, K., Lu, Y., … Ullah, H. (2021). Efficient adsorption of Cr (VI) from aqueous environments by phosphoric acid activated eucalyptus biochar. *Journal of Cleaner Production*, 286, 124964. doi: 10.1016/j.jclepro.2020.124964

[15] Gęca, M., Wiśniewska, M., & Nowicki, P. (2022). Biochars and activated carbons as adsorbents of inorganic and organic compounds from multicomponent systems – A review. *Advances in Colloid and Interface Science*, 305, 102687. doi: 10.1016/j.cis.2022.102687

[16] Saadi, A. S., Bousba, S., Riah, A., Belghit, M., Belkhalfa, B., & Barour, H. (2024). Efficient synthesis of magnetic activated carbon from oak pericarp for enhanced dye adsorption: A one-step approach. *Desalination and Water Treatment*, 319, 100420. doi: 10.1016/j.dwt.2024.100420

[17] Quyen, N. D. V., Tuyen, T. N., Khieu, D. Q., Tin, D. X., Diem, B. T. H., Nhung, N. T. A., … Thu, N. H. N. (2025). The Composite of Activated Carbon/Magnetic Iron Oxide: Synthesis, Isothermal, and Kinetic Studies of Ciprofloxacin and Tetracycline Adsorption From a Binary-Component Solution. *Journal of Nanotechnology*, 2025(1). doi: 10.1155/jnt/2756348

[18] Qu, J., Shi, J., Wang, Y., Tong, H., Zhu, Y., Xu, L., … Zhang, Y. (2022). Applications of functionalized magnetic biochar in environmental remediation: A review. *Journal of Hazardous Materials*, 434, 128841. doi: 10.1016/j.jhazmat.2022.128841

[19] Wang, R., Li, X., Nie, Z., Zhao, Y., & Wang, H. (2021). Metal/Metal Oxide Nanoparticles-Composited Porous Carbon for High-Performance Supercapacitors. *Journal of Energy Storage*, 38, 102479. doi: 10.1016/j.est.2021.102479

[20] Wu, Z., Zhang, H., Ali, E., Shahab, A., Huang, H., Ullah, H., & Zeng, H. (2023). Synthesis of novel magnetic activated carbon for effective Cr(VI) removal via synergistic adsorption and chemical reduction. *Environmental Technology & Innovation*, 30, 103092. doi: 10.1016/j.eti.2023.103092

[21] Yağmur, H. K., & Kaya, İ. (2021). Synthesis and characterization of magnetic ZnCl2-activated carbon produced from coconut shell for the adsorption of methylene blue. *Journal of Molecular Structure*, 1232, 130071. doi: 10.1016/j.molstruc.2021.130071

[22] Bentahar, S., Dbik, A., Khomri, M. El, Messaoudi, N. El, & Lacherai, A. (2017). Adsorption of methylene blue, crystal violet and congo red from binary and ternary systems with natural clay: Kinetic, isotherm, and thermodynamic. *Journal of Environmental Chemical Engineering*, 5(6), 5921–5932. doi: 10.1016/j.jece.2017.11.003

[23] Wang, J., & Guo, X. (2020). Adsorption isotherm models: Classification, physical meaning, application and solving method. *Chemosphere*, 258, 127279. doi: 10.1016/j.chemosphere.2020.127279

[24] Yeung, P.-T., Chung, P.-Y., Tsang, H.-C., Cheuk-On Tang, J., Yin-Ming Cheng, G., Gambari, R., … Lam, K.-H. (2014). Preparation and characterization of bio-safe activated charcoal derived from coffee waste residue and its application for removal of lead and copper ions. *RSC Advances*, 4(73), 38839. doi: 10.1039/C4RA05082G

[25] Jamnongkan, T., Intaramongkol, N., Kanjanaphong, N., Ponjaroen, K., Sriwiset, W., Mongkholrattanasit, R., … Huang, C.-F. (2022). Study of the Enhancements of Porous Structures of Activated Carbons Produced from Durian Husk Wastes. *Sustainability*, 14(10), 5896. doi: 10.3390/su14105896

[26] Nascimento, V. X., Schnorr, C., Lütke, S. F., Da Silva, M. C. F., Machado Machado, F., Thue, P. S., … Dotto, G. L. (2023). Adsorptive Features of Magnetic Activated Carbons Prepared by a One-Step Process towards Brilliant Blue Dye. *Molecules*, 28(4), 1821. doi: 10.3390/molecules28041821

[27] Costa, L. F., Ruotolo, L. A. M., Ribeiro, L. S., Pereira, M. C., Camargo, E. R., & Nogueira, F. G. E. (2021). Low-cost magnetic activated carbon with excellent capacity for organic adsorption obtained by a novel synthesis route. *Journal of Environmental Chemical Engineering*, 9(2), 105061. doi: 10.1016/j.jece.2021.105061

[28] Yadav, M. S., Singh, N., & Bobade, S. M. (2020). VxOy nanoparticles and activated charcoal based nanocomposite for supercapacitor electrode application. *Ionics*, 26(5), 2581–2598. doi: 10.1007/s11581-019-03345-2

[29] Abdulhameed, A. S., Al Omari, R. H., Althahban, S., Jazaa, Y., Abualhaija, M., & Algburi, S. (2025). Green vegetable waste composited with chitosan as a bioadsorbent for effective removal of methylene blue dye from water: Insight into physicochemical and adsorption characteristics. *Biomass and Bioenergy*, 193, 107528. doi: 10.1016/j.biombioe.2024.107528

[30] Ma, M., Ying, H., Cao, F., Wang, Q., & Ai, N. (2020). Adsorption of congo red on mesoporous activated carbon prepared by CO2 physical activation. *Chinese Journal of Chemical Engineering*, 28(4), 1069–1076. doi: 10.1016/j.cjche.2020.01.016

[31] Sudarsan, S., Murugesan, G., Varadavenkatesan, T., Vinayagam, R., & Selvaraj, R. (2025). Efficient adsorptive removal of Congo Red dye using activated carbon derived from Spathodea campanulata flowers. *Scientific Reports*, 15(1), 1831. doi: 10.1038/s41598-025-86032-9

[32] Li, K., Ma, S., Xu, S., Fu, H., Li, Z., Li, Y., … Du, J. (2021). The mechanism changes during bisphenol A degradation in three iron functionalized biochar/peroxymonosulfate systems: The crucial roles of iron contents and graphitized carbon layers. *Journal of Hazardous Materials*, 404, 124145. doi: 10.1016/j.jhazmat.2020.124145

[33] Sun, L., Gong, Y., Li, D., & Pan, C. (2022). Biomass-derived porous carbon materials: synthesis, designing, and applications for supercapacitors. *Green Chemistry*, 24(10), 3864–3894. doi: 10.1039/D2GC00099G

[34] Mayangsari, N. E., Ramadani, T. A., Rachman, F., Juniani, A. I., Hendriatiningsih, S. L., & Ashifa, N. A. (2026). Study on methyl orange adsorption by Fe3O4@SiO2 decorated chitosan schiff base: Insights from kinetics, thermodynamics and response surface methodology for optimization. *Chemical Physics Impact*, 12, 101077. doi: 10.1016/j.chphi.2026.101077

[35] Ali, A. A., & Abdul-Hameed, H. M. (2025). Synthesis and characterization of magnetic activated carbon manufactured from palm stones by physical activation to remove lead from aqueous solution. *Desalination and Water Treatment*, 321, 100951. doi: 10.1016/j.dwt.2024.100951

[36] Gamay, R. A. J., Botecario, P. M. N., Sanchez, P. D. C., & Alvarado, M. C. (2024). Durian (Durio zibenthinus) waste: a promising resource for food and diverse applications—a comprehensive review. *Food Production, Processing and Nutrition*, 6(1), 27. doi: 10.1186/s43014-023-00206-4

[37] Damayanti, A., Wulansarie, R., Bahlawan, Z. A. S., Suharta, Royana, M., Basuki, M. W. N. M., … Andri, A. L. (2023). Effects of Phosphate and Thermal Treatments on the Characteristics of Activated Carbon Manufactured from Durian (Durio zibethinus) Peel. *ChemEngineering*, 7(5), 75. doi: 10.3390/chemengineering7050075

[38] Gong, Z.-X., Steven, M., Chen, Y.-T., Huo, L.-Z., Xu, H., Guo, C.-F., … Luo, X.-P. (2024). High adsorption to methylene blue based on Fe_3O_4–N-banana-peel biomass charcoal. *RSC Advances*, 14(35), 25619–25628. doi: 10.1039/D4RA04973J

[39] Yağmur, H. K., Acer, B., & Özdaş, R. (2025). Using of mesoporous activated carbon obtained by chemical activation of laurel fruit seeds for cationic dye removal. *Applied Physics A*, 131(5), 376. doi: 10.1007/s00339-025-08457-3

[40] Joshy, D., Chakko, S., Ismail, Y. A., & Periyat, P. (2021). Surface basicity mediated rapid and selective adsorptive removal of Congo red over nanocrystalline mesoporous CeO_2. *Nanoscale Advances*, 3(23), 6704–6718. doi: 10.1039/D1NA00412C

[41] Donohue, M. D., & Aranovich, G. L. (1998). Classification of Gibbs adsorption isotherms. *Advances in Colloid and Interface Science*, 76–77, 137–152. doi: 10.1016/S0001-8686(98)00044-X

[42] Liu, Z., Zhang, J., Zhang, L., Guan, Y., Ji, H., Zhang, Y., & Gao, H. (2023). Efficient removal of Congo red and methylene blue using biochar from Medulla Tetrapanacis modified by potassium carbonate. *Bioresource Technology*, 376, 128912. doi: 10.1016/j.biortech.2023.128912

[43] Ntuli, T. D., Mongwe, T. H., Sikeyi, L. L., Mkhari, O., Coville, N. J., Nxumalo, E. N., & Maubane-Nkadimeng, M. S. (2021). Removal of hexavalent chromium via an adsorption coupled reduction mechanism using olive oil derived carbon nano-onions. *Environmental Nanotechnology, Monitoring & Management*, 16, 100477. doi: 10.1016/j.enmm.2021.100477

[44] Huong Do, T., Nguyen, N. P. N., Mai, X. T., Tran, T. H., Dung Nguyen, Q., & Vuong, T. X. (2026). Hierarchically porous activated carbon derived from *Lansium domesticum* peel *via* hydrothermal-H_3PO_4 activation for enhanced methylene blue removal: adsorption behavior, advanced modeling and mechanistic insights. *RSC Advances*, 16(30), 28004–28035. doi: 10.1039/D6RA02695H

[45] Efimova, N. V., Krasnopyorova, A. P., Yuhno, G. D., Sofronov, D. S., & Rucki, M. (2021). Uptake of Radionuclides 60Co, 137Cs, and 90Sr with α-Fe2O3 and Fe3O4 Particles from Aqueous Environment. *Materials*, 14(11), 2899. doi: 10.3390/ma14112899

[46] Peighambardoust, S. J., Rezaei-Aghdam, S., Sakhaei Niroumand, J., Mohammadzadeh Pakdel, P., & Sillanpää, M. (2025). Efficient methylene blue elimination from water media by nanocomposite adsorbent-based carboxymethyl cellulose-grafted poly(acrylamide)/magnetic biochar decorated with ZIF-67. *RSC Advances*, 15(39), 32407–32423. doi: 10.1039/D5RA03796D

[47] Ali, H., & Ismail, A. M. (2023). Fabrication of Magnetic Fe3O4/Polypyrrole/Carbon Black Nanocomposite for Effective Uptake of Congo Red and Methylene Blue Dye: Adsorption Investigation and Mechanism. *Journal of Polymers and the Environment*, 31(3), 976–998. doi: 10.1007/s10924-022-02663-3

[48] Liu, Y. (2008). New insights into pseudo-second-order kinetic equation for adsorption. *Colloids and Surfaces A: Physicochemical and Engineering Aspects*, 320(1–3), 275–278. doi: 10.1016/j.colsurfa.2008.01.032

[49] Foroutan, R., Peighambardoust, S. J., Esvandi, Z., Khatooni, H., & Ramavandi, B. (2021). Evaluation of two cationic dyes removal from aqueous environments using CNT/MgO/CuFe2O4 magnetic composite powder: A comparative study. *Journal of Environmental Chemical Engineering*, 9(2), 104752. doi: 10.1016/j.jece.2020.104752

[50] Bagotia, N. (2025). Regeneration strategies for exhausted adsorbents used in water treatment - A critical review. *Journal of Water Process Engineering*, 69, 106560. doi: 10.1016/j.jwpe.2024.106560